Teleoperation in cluttered environments using wearable haptic feedback

Joao Bimbo[1], Claudio Pacchierotti[2], Marco Aggravi[3], Nikos Tsagarakis[1], and Domenico Prattichizzo[1,3]

***Abstract*— Robotic teleoperation in cluttered environments is attracting increasing attention for its potential in hazardous scenarios, disaster response, and telemaintenance. Although haptic feedback has been proven effective in such applications, commercially-available grounded haptic interfaces still show significant limitations in terms of workspace, safety, transparency, and encumbrance. For this reason, we present a novel robotic teleoperation system with wearable haptic feedback for telemanipulation in cluttered environments. The slave system is composed of a soft robotic hand attached to a 6-axis force sensor, which is fixed to a 6-degrees-of-freedom robotic arm. The master system is composed of two wearable vibrotactile armbands and a Leap Motion. The armbands are worn on the upper arm and forearm, and convey information about collisions on the robotic arm and hand, respectively. The position of the manipulator and the grasping configuration of the robotic hand are controlled by the user's hand pose as tracked by the Leap Motion. To validate our approach, we carried out a human-subject telemanipulation experiment in a cluttered scenario. Twelve participants were asked to teleoperate the robot to grasp an object hidden between debris of various shapes and stiffnesses. Haptic feedback provided by our wearable devices significantly improved the performance of the considered telemanipulation tasks. All subjects but one preferred conditions with wearable haptic feedback.**

I. INTRODUCTION

The field of robotic teleoperation has advanced significantly in the last decades and promising results have been achieved in several telemanipulation tasks, such as space exploration [1], minimally invasive surgery [2], sort and segregation of waste [3], telemaintenance [4], and micromanipulation [5]. As teleoperation systems become more sophisticated and flexible, the environments and applications in which they can be employed become less structured and predictable. In this respect, robotic teleoperation in cluttered environments is attracting increasing attention for its potential in hazardous scenarios [3], [6] and disaster response [7], [8], [9]. In fact, being able to intuitively manipulate objects in a remote environment cluttered with waste, debris, or hazardous materials could significantly extend the application range of robotic teleoperation systems. For example, Jurmain et al. [8] designed a remotely operated robot for bio-event disaster response, called HazBot. It is composed of a mobile robot equipped with a 6-degrees-of-freedom (6-DoF) manipulator. The manipulator incorporates a parallel jaw gripper with a 60 pound squeeze force and a gas detector to aid in material identification. Murphy et al. [9] evaluated the use of three Unmanned Marine Vehicles (UMV) in two areas damaged by the tsunami following the 2011 Tohoku Earthquake. The employed UMVs had a multi-beam imaging sonar, video, and a gripper. More recently, Farraj et al. [3] proposed a shared-control architecture for remote manipulation of nuclear waste. A visual-based autonomous algorithm regulates a subset of the gripper's degrees of freedom to ease the approach towards the target object. Simultaneously, the human operator steers the gripper along with the remaining null-space directions through a grounded haptic interface. Haptic feedback has been proven to play a key role in enhancing the performance of robotic telemanipulation systems in a wide range of applications, including suturing simulation [10], microassembly [11], [12], [13], microneedle positioning [14], guidance [15], telepresence [16], and palpation [17], [18]. Haptic feedback has proven to enhance the performance of these systems in terms of completion time [10], [19], accuracy [10], [20], and peak and mean exerted force [18], [19], [21].

Current haptic technology for teleoperation and telemanipulation is indeed very advanced, but it is usually neither wearable nor portable. Nonetheless, the use of wearable haptic interfaces in telemanipulation can significantly improve the comfort, workspace, and range of application of these systems [22], [23], [24]. Moreover, wearable interfaces can easily enable the engaging of multi-contact interactions and operations. Finally, ungrounded haptic devices have also been proven to guarantee the stability and safety of haptic-enabled teleoperation loops [13], [19], [25].

To this end, a variety of new wearable haptic devices have been developed specifically for teleoperation and virtual interaction applications [26]. In this respect, there is a growing interest in vibrotactile stimuli as an effective and unobtrusive substitute of conventional force feedback. For example, Romano et al. [27] presented a vibrotactile glove that provided tactile cues associated with slippage between a glove and a contact surface. Optical mouse sensors embedded on the glove's surface, sensed the relative motions, and this information was conveyed to the user through vibrating motors placed inside the glove against the user's finger pad. Hayes [28] provided vibrotactile feedback on the hand for haptic-enabled music performances. The author integrated two vibrating motors on the palm to recreate the vibrations produced by an acoustic instrument. The fingertips are left free to interact with the environment. Kurihara et al. [29] used a vibrotactile armband with four motors to provide haptic intonation of the human elbow joint to resemble the one of a robot. To create a realistic robot-like body sense, the authors provided vibrotactile stimuli built from vibration recordings of real robot actuation, data-driven modeling based on spectral approximation, and vibrotactile rendering to the wearer's elbow joint as a function of its angular velocity. More recently, Brygo et al. [30] used a vibrotactile waistband to provide feedback in teleoperation of humanoid robots. They proved that feeding back the robot's balance state

This research was funded by the European Union FP7/2007-2013, grant n°601165 (WEARHAP) and from the European Union's Horizon 2020 Research and Innovation Programme, grant n°645599 (SOMA).

[1] Dept. of Advanced Robotics, Istituto Italiano di Tecnologia, Italy.
[2] CNRS at Irisa and Inria Rennes Bretagne Atlantique, France.
[3] Dept. of Information Engineering and Mathematics, Univ. of Siena, Italy.

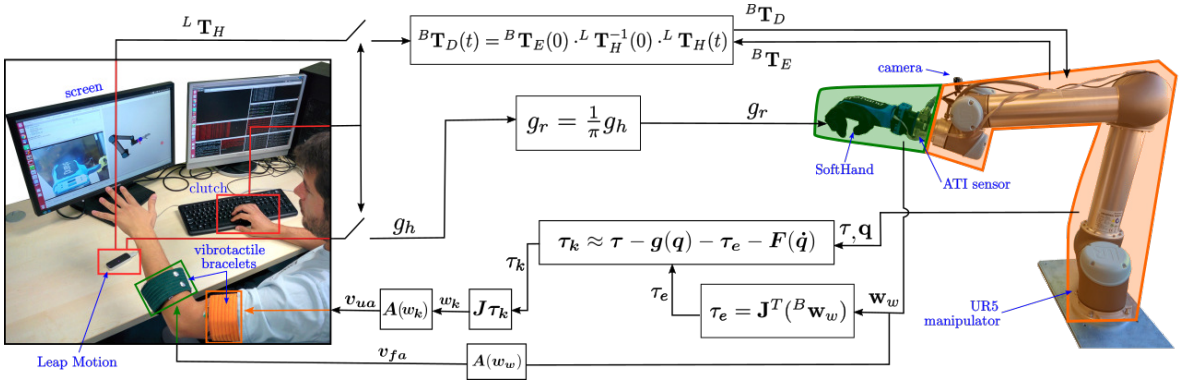

Fig. 1. Haptic-enabled teleoperation system. The slave system is composed of an anthropomorphic IIT/Pisa SoftHand, attached to an ATI Gamma force-torque sensor, which is in turn fixed to a 6-DoF Universal Robot arm. The master system is composed of a Leap Motion controller and two wearable vibrotactile armbands, worn on the upper arm and forearm. The Leap Motion tracks the user's hand pose and commands the position of the manipulator and the grasping configuration of the robotic hand. The armbands on the arm convey information about collisions of the slave hand/wrist system (green patch to green/forearm armband) and slave arm (orange patch to orange/upper arm armband). The amplitude of the vibrotactile feedback is proportional to the collision force. A camera mounted near the manipulator's end-effector enables the operator to see the environment in front of the robotic hand. A virtual rendering of the robot provides information about its configuration.

through the vibrotactile belt significantly enhances the quality of the teleoperation. Similar systems, featuring different arrangements of vibrotactile actuators across the body, have shown promising results in various applications, such as robot-assisted surgery [31], guidance of visually-impaired people [32], virtual reality [33], and enhanced cinematic experiences [34].

This paper presents a novel haptic-enabled telemanipulation system for operation in cluttered environments, shown in Fig. 1. The slave system is composed of an anthropomorphic soft robotic hand attached to a 6-axis force-torque sensor, which is in turn fixed to a 6-DoF robotic arm. The master system is composed of a Leap Motion controller and two wearable vibrotactile armbands, worn on the forearm and upper arm. The Leap Motion tracks the user's hand pose to control the pose of the manipulator and the grasping configuration of the robotic hand. The armband on the forearm conveys information about collisions of the slave hand/wrist system (green patch to green armband, see Fig. 1), whereas the armband on the upper arm conveys information about collisions of the slave arm (orange patch to orange armband). The amplitude of the vibrotactile feedback relayed by the armbands is proportional to the interaction force of the collision. A camera mounted near the manipulator's end-effector enables the operator to see the environment in front of the robotic hand. To the best of our knowledge, this is the first work where a multi-point wearable haptic system is used in robotic teleoperation to convey information about the location and stiffness of collisions at the slave side.

To validate our system, we carried out a human subjects telemanipulation experiment in a cluttered scenario. Twelve participants were asked to control the motion of the robotic manipulator to grasp an object hidden between debris of various shapes and stiffnesses.

II. Teleoperation System

A. Master system

The master system is composed of a vision-based Leap Motion tracker and two custom made wearable vibrotactile armbands. Operators are asked to wear one armband on the forearm and one on the upper arm (see left-hand side of Fig. 1).

The Leap Motion is a small USB peripheral device that uses two monochromatic IR cameras and three infrared LEDs to track the position of the fingertips and wrist in 3-D space. It observes a hemispherical area up to a distance of 1 m with an accuracy up to 0.01 mm. The hand grasping configuration, i.e., how closed the hand is, is measured by considering the radian angle g_h between the index finger's distal phalanx direction $\hat{h}_{i34}$ and the hand direction $\hat{h}_d$ (see Fig. 2),

$$g_h = \cos^{-1}\left(\hat{h}_{i34} \cdot \hat{h}_d\right). \quad (1)$$

The haptic armbands are composed of four Precision Microdrives 307-100 Pico Vibe 9mm vibration motors (A in Fig. 2), which have an effective vibration frequency range of 100-280 Hz, an Arduino Mini Pro 3.3 V, a 3.7 V LiPo battery, and a RN-42 Bluetooth 2.1 antenna. The electronics and battery are embedded into a 3D-printed case (B), and the same is done for each motor. The devices have the form of an elastic wristband with a VELCRO strap, which can be covered by a colored elastic band (C). When worn, the motors are positioned evenly around the arm, at 90 degrees from each other, allowing the system to provide directional information about the collisions. The Precision Microdrives motors we used do not enable the independent control of amplitude and frequency. Changing the input voltage in the range $[1.2;\ 3.6]$ V produces vibrations with amplitude and frequency in the range of $[2.75\ \ 7.25]$ g and $[100\ \ 260]$ Hz, respectively. More information can be found in the motor's data sheet. The microcontroller receives a four byte packet every 200 ms and sets the vibration of each motor accordingly.

B. Slave system

The slave system is composed of the anthropomorphic Pisa/IIT SoftHand soft robotic hand, attached to a 6-axis ATI Gamma force-torque sensor, which is in turn fixed to a 6-DoF Universal Robot 5 manipulator. A standard webcam is attached to the robot's wrist, showing the environment in front of the robotic hand.

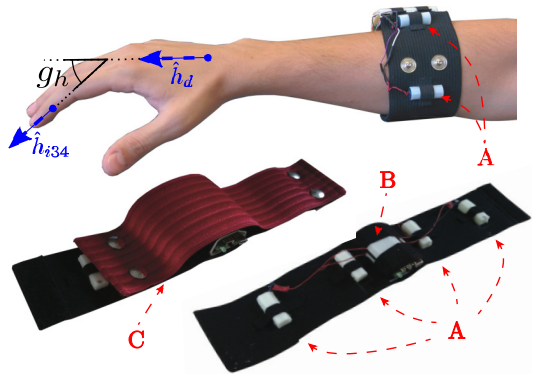

Fig. 2. Wearable haptic armband. The device is equipped with four vibrating motors (A), its electronics is enclosed in a 3D-printed case (B), and it can be covered by an elastic colored band (C). When worn, the motors are positioned evenly around the arm, at 90 degrees from each other.

1) Pisa/IIT SoftHand: The robotic hand has 19 joints, but uses only one actuator to activate its adaptive synergy [35]. The index, middle, ring, and little fingers have four phalanges, while the thumb has three. The palm is connected to a flange, to be fixed at the manipulator's end-effector, through a compliant wrist allowing for three passively compliant degrees of freedom. The motor of the hand is driven by commanding a grasping variable $g_r \in [0, 1]$, which sets the hand closure.

2) Force-torque sensor: The ATI Gamma is a six-axis force-torque sensor with a diameter of 75.4 mm and a weight of 0.255 kg. The forces registered by the force-torque sensor are used to detect collisions between the robotic hand/wrist system (green patch in Fig. 1) and the environment.

3) Universal Robot 5 6-DoF manipulator: The 6-DoF manipulator is able to move the end-effector at up to 1 m/s and each joint at 180 deg/s. Its repeatability is ± 0.1 mm for quick-precision handling with a maximum payload of 5 kg.

The robotic manipulator joints are controlled using velocity commands $\dot{\boldsymbol{q}} \in \mathbb{R}^6$. These velocities are calculated using the Levenberg-Marquardt inverse kinematics solver available within the Kinematics and Dynamics Library (KDL) [36]. This method displayed better results than the Jacobian pseudo-inverse, particularly in the vicinity of singular configurations, where it behaved more stably [37]. When a desired end-effector pose (position and orientation), with respect to the robot base, is commanded, the change in joint angles is calculated by

$$\Delta \boldsymbol{q} = (\boldsymbol{J}^T \boldsymbol{J} + \lambda \cdot \boldsymbol{I})^{-1} \boldsymbol{J}^T \boldsymbol{e}, \tag{2}$$

where $\boldsymbol{J} \in \mathbb{R}^{6\times 6}$ is the manipulator Jacobian matrix, λ is the learning rate, and $\boldsymbol{e}$ is the weighted difference in translation and rotation between the current end-effector pose ${}^B\boldsymbol{T}_E \in \mathrm{SE}(3)$ and the desired pose ${}^B\boldsymbol{T}_D \in \mathrm{SE}(3)$ [38]. By setting the velocities in the control loop $\dot{\boldsymbol{q}} = K_p \cdot \Delta \boldsymbol{q}$, this method acts as a proportional controller with gain K_p, tracking the desired pose.

Motor currents are accessible and are used to estimate joint torques. An approximation of the joint torques can be obtained from the relationship

$$\tau_i = K_{\tau i} \cdot I_i, \tag{3}$$

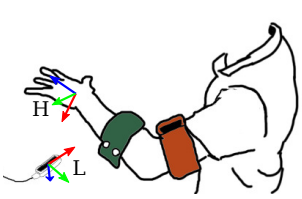

(a) User commanding the robot, Hand frame H and Leap Motion frame L.

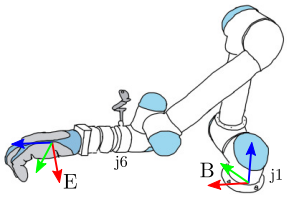

(b) Robot end-effector frame E and Base frame B.

Fig. 3. Coordinate frames used to command the robot end effector pose. Axes x, y, and z shown as red, green, and blue arrows, respectively.

where I_i is the motor current and $K_{\tau i}$ is a constant that approximates the ratio between current and output torque for joint i. It is a product of the motor torque constant, gearbox ratio, and efficiency. To estimate this relationship, the robot was set in gravity compensation mode and moved to arbitrary positions in the workspace. The measured motor currents along with the demanded joint torques to maintain the robot in each posture were recorded and a linear fitting was carried out. $K_{\tau i}$ was found to be 13.2 N·m/A for the first three motors and 9.3 N·m/A for the last three.

III. Methods

A. Motion Control

The desired pose of the robot hand at time t, ${}^B\boldsymbol{T}_D(t)$, is commanded using a mapping between the robot hand and the user's hand, tracked by the Leap Motion. The keyboard works as a clutch. The coordinate frames are shown in Fig. 3. When the space key is pressed, the current pose of the user's hand with respect to the Leap Motion base ${}^L\boldsymbol{T}_H \in \mathrm{SE}(3)$ and the robot's end effector pose with respect to its base ${}^B\boldsymbol{T}_E$ are saved:

$$\begin{aligned} {}^L\boldsymbol{T}_H(0) &= {}^L\boldsymbol{T}_H(t), \\ {}^B\boldsymbol{T}_E(0) &= {}^B\boldsymbol{T}_E(t). \end{aligned} \tag{4}$$

As the user moves the hand, the desired end effector pose is calculated according to Eq. (5), using the poses saved when the user started pressing the clutch, such that their relative motions are equal, i.e. ${}^{E_0}\boldsymbol{T}_D = {}^{H_0}\boldsymbol{T}_H$,

$${}^B\boldsymbol{T}_D(t) = {}^B\boldsymbol{T}_E(0) \cdot {}^L\boldsymbol{T}_H^{-1}(0) \cdot {}^L\boldsymbol{T}_H(t). \tag{5}$$

Differently from [39], where there is a fixed mapping between the Leap Motion frame L and the robot base B, our mapping allows the robot to be commanded in a more natural way while looking at the camera: if the user moves his hand in the z direction of the H frame, the robot will move along the z direction of its frame E (see Fig. 3). Moreover, this mapping and clutching approach allows the user to start the motion with the hand at an arbitrary position with respect to the Leap Motion, enabling him to pause, move to a more comfortable or suitable position, and then resume control of the robot. This approach also solves the problem of limited workspace on the master side. Besides, the scaling of the robot motion with respect to the user's hand can be easily changed, enlarging or reducing the workspace of the manipulator with respect to the workspace of the Leap Motion. However, in the following experiments, the motion scaling was kept to 1.

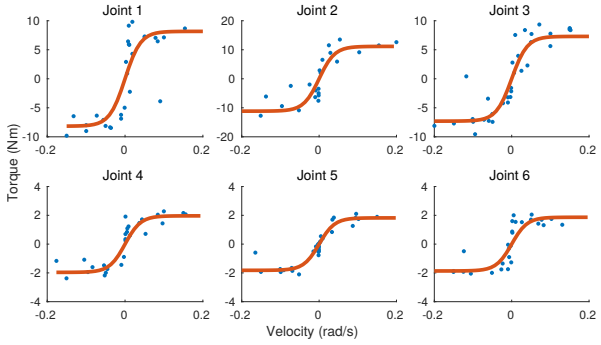

Fig. 4. Estimation of dynamic friction torques for each joint. Measurements are reported in blue, fitting of a sigmoid function is reported in orange.

To match the grasping configuration of the operator's hand to the robot, we define the input commanded to the hand DC motor as

$$g_r = \frac{1}{\pi} g_h, \tag{6}$$

where a command of 0% closure is sent when the index is parallel with the palm direction and 100% closure is commanded when the index finger is bent 180° (see Eq. (1) and Fig. 2).

B. Haptic feedback

Haptic feedback is provided through the vibrotactile armbands worn on the forearm and upper arm, as described in Sec. II-A.

1) Wrist/hand system: Vibrations elicited on the forearm are obtained from the forces measured by the force-torque (FT) sensor mounted at the robot's wrist (see Fig. 1). The interaction wrench $\boldsymbol{w_w} = [\boldsymbol{f_w}^T \quad \boldsymbol{\tau_w}^T]^T \in \mathbb{R}^6$ between the wrist/hand system (green patch in Fig. 1) and the environment is calculated by subtracting the effect of gravity $\boldsymbol{w_g}$ on the robot hand to the measured wrench $\boldsymbol{w}$,

$$\boldsymbol{f_g} = ({}^B\boldsymbol{R}_E)^{-1} \cdot [0, 0, g \cdot m_H]^T, \tag{7}$$

$$\boldsymbol{w_g} = \begin{bmatrix} \boldsymbol{f_g} \\ \boldsymbol{r_H} \times \boldsymbol{f_g} \end{bmatrix}, \quad \boldsymbol{w_w} = (\boldsymbol{w} - \boldsymbol{w_g}), \tag{8}$$

where ${}^B\boldsymbol{R}_E$ is the rotation part of transformation ${}^B\boldsymbol{T}_E$, $g \cdot m_H$ is the weight of the robot hand, and $\boldsymbol{r_H}$ is the vector from the sensor origin to the robot hand's center of gravity (see Fig. 3).

2) Robotic manipulator: Interaction forces on the robot body can be obtained by analysing joint currents [40]. Joint torques are estimated using Eq. (3) and result from the manipulator equation

$$\boldsymbol{M}(\boldsymbol{q})\ddot{\boldsymbol{q}} + \boldsymbol{C}(\boldsymbol{q}, \dot{\boldsymbol{q}})\dot{\boldsymbol{q}} + \boldsymbol{F}(\dot{\boldsymbol{q}}) + \boldsymbol{g}(\boldsymbol{q}) + \boldsymbol{\tau_e} + \boldsymbol{\tau_k} = \boldsymbol{\tau}, \tag{9}$$

where $\boldsymbol{q}$ is the vector of joint angles, $\boldsymbol{M}$ is the inertia matrix, $\boldsymbol{C}$ is the vector of Coriolis and centrifugal terms, $\boldsymbol{F}$ is the vector of dynamic friction torques, $\boldsymbol{g}$ is the vector of gravity joint torques, $\boldsymbol{\tau_e}$ denotes the torques resulting from interactions at the robot's end-effector, and $\boldsymbol{\tau_k}$ is the vector of torques caused by interactions between the environment and the robot links [41].

If velocities and accelerations are kept sufficiently low, then

$$\boldsymbol{\tau_k} \approx \boldsymbol{\tau} - \boldsymbol{g}(\boldsymbol{q}) - \boldsymbol{\tau_e} - \boldsymbol{F}(\dot{\boldsymbol{q}}). \tag{10}$$

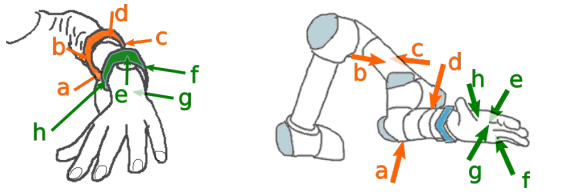

Fig. 5. Mapping of collision locations on the robot arm to vibrotactile motors on the armbands.

Since the wrench at the end effector $\boldsymbol{w_w}$ can be readily obtained from the mounted force-torque sensor (see Sec. III-B.1), the torque $\boldsymbol{\tau_e}$ that it generates on each joint is obtained by applying the principle of virtual work [42],

$$\boldsymbol{\tau_e} = \boldsymbol{J}^T({}^B\boldsymbol{w_w}). \tag{11}$$

The torques resulting from dynamic friction $\boldsymbol{F}(\dot{\boldsymbol{q}})$ can be approximated using a smoother Coulomb friction model. This function was obtained by fitting a sigmoid function $F_i(\dot{q}_i)$ to the additional torques measured at each joint during movement [43]:

$$F_i(\dot{q}_i) = \frac{2 \cdot L}{(1 + e^{-50 \cdot \dot{q}_i})} - L. \tag{12}$$

Fig. 4 shows the fitting of function F_i for each robot joint. The obtained L values for each joint were 7.8, 11.0, 8.0, 2.0, 2.0, and 2.0 respectively. This smoother version of the Coulomb model was used instead of the standard discontinuous model because the measurement of joint speeds is subject to noise, which would lead to the estimation of larger friction forces when the robot is nearly static.

The vector of external torques $\boldsymbol{\tau_k}$ can then be mapped into a wrench $\boldsymbol{w_k}$ in the end-effector reference frame:

$$\boldsymbol{w_k} = \begin{bmatrix} ({}^B\boldsymbol{R}_E)^{-1} & \boldsymbol{0} \\ \boldsymbol{0} & ({}^B\boldsymbol{R}_E)^{-1} \end{bmatrix} \cdot \boldsymbol{J} \cdot \boldsymbol{\tau_k}. \tag{13}$$

3) Modulation of vibrations: Collisions with the environment can be discriminated between arm and hand and conveyed to the user through the vibrotactile armbands. If the estimated interaction force is above a threshold of 5 N, the respective vibrotactile motors are activated to communicate to the user the direction and intensity of the collision. This threshold value is used to prevent spurious vibrations originating from modelling errors and noise. Impacts at the robot body $\boldsymbol{w_k}$ are relayed to the armband on the upper arm, whereas contacts at the robot hand and wrist $\boldsymbol{w_w}$ are transmitted to the forearm bracelet (see Fig. 1). For each armband $l \in \{\text{upper arm } (ua), \text{forearm } (fa)\}$, the voltage input $\boldsymbol{v}_l = [v_1, v_2, v_3, v_4]$ on each motor is driven by the mapping function $\boldsymbol{A}(\boldsymbol{w})$.

$$\boldsymbol{v}_l = \boldsymbol{A}(\boldsymbol{w}) = 15 \cdot \begin{bmatrix} +\max(0, f_x) \\ -\min(0, f_x) \\ +\max(0, f_y) \\ -\min(0, f_y) \end{bmatrix} \tag{14}$$

This function maps and scales the force components of $\boldsymbol{w} = [f_x \ f_y \ f_z \ m_x \ m_y \ m_z]^T$ to the corresponding vibrotactile motors placed around each of the armbands (see Fig. 5). For example, a collision on the dorsal side of the robot hand (position **e** in Fig. 5) will induce vibrations on the forearm's

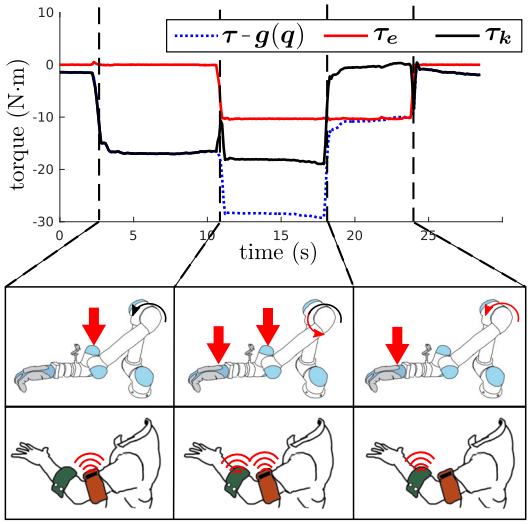

Fig. 6. Interaction detection at the hand/wrist and arm. Torques on the 3rd joint are plotted. First, a force is applied on the robot arm, then simultaneously on the robot arm and hand. Finally, only a force at the robot hand is applied. The red line shows the torque resulting from interactions at the hand/wrist and the black line shows the torque from interactions on the arm. The blue dotted line is the measured joint torque, compensated for gravity

bracelet motor placed at the dorsal side of the user's wrist, whereas a negative force in that direction will make the opposite motor vibrate. When a collision with the robot body occurs, the vibrating motor depends on the current posture of the robot. In the example of Fig. 5, a collision in the direction of **c**, will induce vibrations in the posterior side of the human upper arm, suggesting the user to move the arm away from the obstacle, by performing an arm extension movement. The scaling factor for $\boldsymbol{A}$ was chosen to maximize the just-noticeable difference for the considered range of forces and fit the vibromotors specifications (see Sec. II-A).

4) Validation: Fig. 6 shows an example of the proposed collision detection method. A weight is placed at the robot's 4th link, causing an increase of the joint torque $\boldsymbol{\tau_k}$ (left side). Then, a second weight is placed on the robot hand, which causes an increase of $\boldsymbol{\tau_e}$, while $\boldsymbol{\tau_k}$ remains approximately constant (center). Finally, the first weight is removed, and the torque measured at the joint is due solely to the weight on the wrist (right side).

This procedure generated vibrations at the upper arm between $t = 2$ s and $t = 18$ s and vibrations at the forearm between $t = 11$ s and $t = 24$ s (at locations **d** and **e** in Fig. 5, respectively).

IV. Experimental Evaluation

A. Setup

The experimental setup is composed of the integrated haptic-enabled telemanipulation system shown in Fig. 1 and described in Sec. II. The remote environment, shown in Fig. 7, is composed of several objects of different sizes, shapes, and stiffnesses, placed disorderly on a 1.02×0.75 m wooden table. The base of the slave robot is attached directly to the table.

In addition to the haptic feedback and motion/grasping control capabilities detailed in Sec. II, the system also provides the human operator with visual feedback through a camera

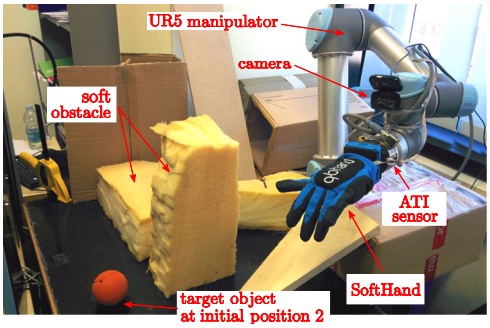

(a) Remote environment with soft obstacles between the slave robot and the target object to grasp.

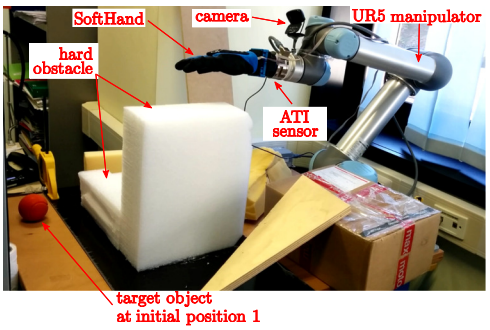

(b) Remote environment with hard obstacles between the slave robot and the target object to grasp.

Fig. 7. Remote environment cluttered with different obstacles. The task consists in grasping and lifting a red soft ball which was hidden by either soft or hard obstacles. Moreover, we carried out the grasping task placing the ball in two different initial positions.

attached to the robot's wrist. A virtual rendering created using RViz also shows the robot's current configuration robot and the approximate location of the target object to grasp. This virtual rendering does not show any obstacle. The camera view and rendering are shown in a screen placed in front of the user, as shown in Figs. 1 and 8.

B. Subjects

Twelve participants took part in the experiment, including 2 women and 10 men (age 24 – 38), all right-hand dominant. Three of them had previous experience with wearable haptic interfaces. None of the participants reported any deficiencies in their haptic perception abilities. The experimenter explained the procedure and spent about three minutes adjusting the setup to be comfortable. No practice trial was allowed.

C. Methods

The task consists in grasping and lifting a red soft ball with diameter of 8 cm, hidden between various obstacles. The

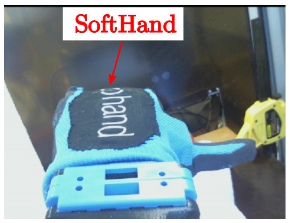

(a) View from the camera.

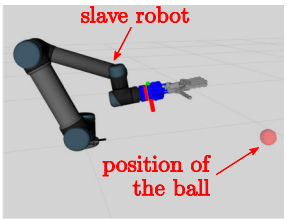

(b) Virtual rendering from RViz.

Fig. 8. Visual information available to the user. (a) image acquired from the camera mounted on the wrist; (b) robot model displaying the current posture and initial location of the target object.

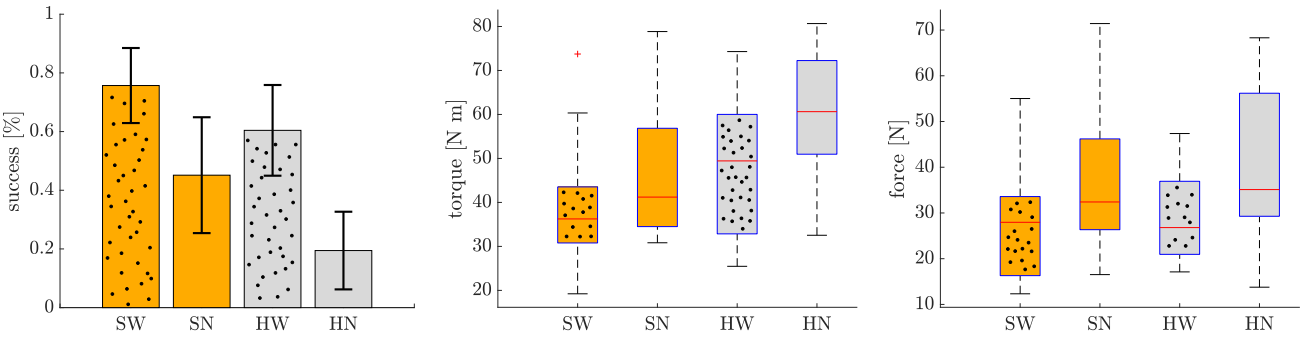

(a) Task success rate (mean ± 95% confidence interval)

(b) Maximum torque $\boldsymbol{\tau_k}$ from the manipulator (boxplot)

(c) Maximum force $\|\boldsymbol{f_w}\|$ from the force-torque sensor (boxplot)

Fig. 9. Results of the human subject experiments. **SW**: Soft obstacles, using haptic feedback, **SN**: Soft obstacles, without haptic feedback, **HW**: Hard obstacles, using haptic feedback, **HN**: Hard obstacles, without haptic feedback,

operator is requested to wear one armband on the forearm, one on the upper arm, and move the slave robot inside the cluttered environment, towards the target ball. The operator receives haptic feedback through the armbands and controls the robotic hand through the Leap Motion, as detailed in Sec. II.

We considered two different *feedback conditions*: with (W) and without (N) vibrotactile haptic feedback. In condition W, the human operator received haptic information about the collisions of the robot with the environment through the vibrotactile armbands, as described in Sec. III. In condition N, the vibrotactile armbands were not active. We also considered two different *environmental conditions*: soft (S) or hard (H) obstacles. In condition S, the main obstacles between the initial position of the slave robot and the target object were made of deformable foam rubber, as shown in Fig. 7a. In condition H, the same obstacles were made of hard polystyrene, as shown in Fig. 7b. Finally, we carried out our grasping tasks placing the target ball in two different positions, requiring the user to complete two very different motions. We ended up with 2 (feedback conditions) $\times$ 2 (environmental conditions) $\times$ 2 (target positions) = 8 different experimental conditions. Each subject carried out at least 8 repetitions of the task, for a total of 152 trials. Trials were randomized to avoid any learning effect. Data from the same experimental condition and subject were averaged before the analysis [20]. Before starting the experiment, the experimenter checked if the subject was able to correctly recognize the vibration of different motors and bracelets. Each motor was made vibrate separately, and the subject was asked to determine from which bracelet and motor the vibration originated. Subjects replied correctly 92% of the times.

A video with trials in all experimental conditions is available as supplemental material and at http://goo.gl/RLn0mX.

D. Results

To evaluate the effectiveness of our system in a cluttered environment and the usefulness of wearable haptic feedback in such situations, we evaluated (1) the success rate in completing the grasping task, (2) the maximum torques generated by the collision of the manipulator with the environment, (3) the maximum forces generated by the collision of the hand/wrist system with the environment, and (4) the completion time. To compare the different metrics, we ran two-way repeated-measures ANOVA tests on the data. Feedback condition (W vs. N) and environmental condition (S vs. H) were treated as within-subject factors. All data passed the Shapiro-Wilk normality test.

Figure 9a shows the average success rate in completing the given grasping task. A task was considered successfully completed when the slave robot was able to grasp the ball and lift it from the ground. A failure was registered when the Universal Robot arm went into protective mode due to high forces or torques caused by strong collisions. Forces at the end-effector above 150 N, or torques exceeding 42 Nm on any of the first three joints, or torques exceeding 10 Nm on the last three joints, triggered the robot to go into protective mode. The external torque required to go into protective mode is also dependent on its direction. For example, if the second joint of the robot is producing a torque of 20 Nm to oppose gravity, the robot will go into protective mode if a collision with the environment generates a torque in excess of 22 Nm if the direction of that torque is the same as the gravity torque, and of 62 Nm if the direction is opposite to gravity. Data was transformed using the arcsin transformation, as it is indicated for rates [44]. The ANOVA test revealed a statistically significant change in the task success for both the feedback condition ($F(1, 11) = 2.795$, $p = 0.001$) and the environment ($F(1, 11) = 5.713$, $p = 0.036$) variables. The interaction effect between feedback condition and environment was not statistically significant. This result shows that providing haptic feedback significantly increased the success rate of the task. Moreover, as expected, interacting with a stiffer environment produced more failures than interacting with a softer environment.

Figure 9b shows the maximum registered torques $\max(\|\boldsymbol{\tau_k}\|)$, generated by the collisions of the manipulator with the environment (see Eq. (10)). As a high peak force during the task could lead to a damage of the robot and the environment, a low value of this metric denotes the best performance. The ANOVA test revealed a statistically significant change in the metric for both the feedback condition ($F(1, 11) = 5.474$, $p = 0.039$) and the environment ($F(1, 11) = 11.788$, $p = 0.006$) variables. The interaction effect between feedback condition and environment was not statistically significant. These results show that providing

haptic feedback significantly reduced the collisions torques at the arm and that, as expected, a stiffer environment produces higher collisions torques.

Figure 9c shows the maximum registered force $\max(\|\boldsymbol{f_w}\|)$, generated by the collisions of the hand/wrist system with the environment (see Eq. (8)). Again, a low value of this metric denotes the best performance. The ANOVA test revealed a statistically significant change in the metric for the feedback condition variable only ($F(1, 11) = 25.933$, $p < 0.001$). The interaction effect between feedback condition and environment was not statistically significant. Haptic feedback improved the performance of the task also for this metric.

Finally, we also measured the completion time, considering only the successful tasks. The ANOVA test indicated no significant difference in the performance among feedback conditions and environments. Average completion time was 105.42 $\pm$ 59.70 s (mean $\pm$ SD).

In addition to the quantitative evaluation reported above, users' experience was also measured. Immediately after the experiment, subjects were asked to report (i) the effectiveness of each feedback condition in completing the given task, (ii) the wearability of the feedback system, and (iii) its intuitiveness using bipolar Likert-type nine-point scales. A Friedman test showed a statistically significant difference for the perceived effectiveness and the intuitiveness variables (W vs. N: effectiveness, 7.25 vs. 3.00, $z = -2.943, p = 0.003$; wearability, 6.83 vs. 7.08, $z = 1.342, p = 0.180$; intuitiveness, 7.00 vs. 3.34, $z = -2.766, p = 0.006$). Finally, subjects were also asked to choose the condition they preferred the most. All subjects but one preferred the condition providing vibrotactile haptic feedback (W). The role of the upper arm armband was particularly appreciated, since the camera only showed the hand and it was therefore not possible to visually check for collisions between the manipulator and the environment. Subjects also appreciated how the vibrations amplitude changed accordingly to the collision force. This information, together with the movement of the slave robot, enabled the subjects to estimate the stiffness of the colliding object.

V. Discussion And Conclusions

In this paper, we presented a teleoperation system for manipulation in cluttered environments. The system tracks the user's hand to guide the robot and grasp an object placed behind obstacles of different shapes and stiffnesses.

When the robot collides with the environment, whether at the hand/wrist, arm links, or both, the collision forces are relayed to the user through a pair of vibrotactile armbands placed at corresponding positions of the user's arm (forearm and upper arm).

In order to evaluate the effectiveness of our approach, we carried out a human-subjects experiment, enrolling 12 subjects. Results showed a significant improvement when using haptic feedback. Compared to the case where no haptic feedback was provided, the rate of success in completing the task increased by 111%. Moreover, when using haptic feedback, the forces exerted by the manipulator on the environment were significantly lower, resulting in a safer system. All subjects but one preferred the conditions providing haptic feedback, considering it effective, unobtrusive, and intuitive. Finally, this study also validates the effectiveness of employing multiple bracelets. 92% of subjects were able to correctly discriminate the vibration of each different motor and bracelet. Furthermore, it was noticeable that subjects did not use haptic feedback only to detect undesired collisions with the environment. In fact, haptic feedback also assisted the users' grasping strategy when approaching the target object: when the palm came in contact with the ball, the vibrations on the forearm notified the user that the ball was ready to be grasped. This was particularly useful when the target object was occluded by the robotic hand.

Fig. 10 shows the trajectory of two representative runs with obstacles of different stiffness (environmental conditions S and H). When colliding with a soft obstacle (condition S, Fig. 10a), users tended to push the obstacle to reach the target object, since the vibrations were slowly increasing (see Eq. (14)). On the other hand, if the collision occurred with a stiffer object (condition H, Fig. 10b), the sudden increase in vibrations made the users adjust the orientation of the hand to avoid any further, and possibly dangerous, collision.

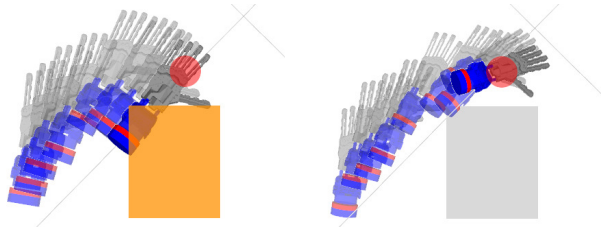

(a) Soft obstacle (b) Hard obstacle

Fig. 10. The object approach strategy varied according to the environment.

In the future, we plan to account for robot dynamics, i.e., extend the approximation in Eq. (10) to also consider $\boldsymbol{M}(\boldsymbol{q})\ddot{\boldsymbol{q}} + \boldsymbol{C}(\boldsymbol{q}, \dot{\boldsymbol{q}})\dot{\boldsymbol{q}}$. Since these components were not taken into account, sudden stops of the robot induced, at times, small spurious vibrations on the bracelets and required the robot to operate at slower speeds. Moreover, using a torque controlled robot would also improve the quality of feedback signals. In this respect, in the future we will employ a KUKA iiwa manipulator. Additional sensors and haptic devices could be added to convey richer information to the user, such as tactile sensors on the robot hand and haptic devices on the user's fingertips. Besides, tracking the user's arm orientation could improve the mapping of vibrations at the upper arm, since there is a degree of redundancy on the human arm. Being able to independently control the amplitude and frequency of the feedback vibrations could also help to provide more informative cues about the collisions. We also plan to use this setup to gain an insight on how humans perform grasps that exploit the environment, with the aim of implementing strategies to execute them autonomously. Finally, we will employ a more sophisticated tracking system, such as the Optitrack V120:Trio system, which will provide a larger workspace at the master side.

REFERENCES

[1] W.-K. Yoon, T. Goshozono, H. Kawabe, M. Kinami, Y. Tsumaki, M. Uchiyama, M. Oda, and T. Doi, "Model-based space robot teleoperation of ets-vii manipulator," *IEEE Transactions on Robotics and Automation*, vol. 20, no. 3, pp. 602–612, 2004.

[2] C. Freschi, V. Ferrari, F. Melfi, M. Ferrari, F. Mosca, and A. Cuschieri, "Technical review of the da vinci surgical telemanipulator," *The International Journal of Medical Robotics and Computer Assisted Surgery*, vol. 9, no. 4, pp. 396–406, 2013.

[3] F. Farraj, N. Pedemonte, and P. Robuffo Giordano, "A visual-based shared control architecture for remote telemanipulation," in *IEEE/RSJ Int. Conf. on Intelligent Robots and Systems*, 2016.

[4] D. Aschenbrenner, M. Fritscher, F. Sittner, M. Krauß, and K. Schilling, *Teleoperation of an Industrial Robot in an Active Production Line*, 2015.

[5] J. Cecil, M. B. R. Kumar, Y. Lu, and V. Basallali, "A review of micro-devices assembly techniques and technology," *The International Journal of Advanced Manufacturing Technology*, vol. 83, no. 9-12, pp. 1569–1581, 2016.

[6] J. P. Trevelyan, S.-C. Kang, and W. R. Hamel, "Robotics in hazardous applications," in *Springer Handbook of Robotics*. Springer, 2008, pp. 1101–1126.

[7] S. Stramigioli, R. Mahony, and P. Corke, "A novel approach to haptic tele-operation of aerial robot vehicles," in *Proc. IEEE Int. Conf. on Robotics and Automation*, 2010, pp. 5302–5308.

[8] J. Jurmain, A. Blancero, J. Geiling, A. Bennett, C. Jones, J. Berkley, M. Vollenweider, M. Minsky, J. Bowersox, and J. Rosen, "Hazbot: Development of a telemanipulator robot with haptics for emergency response." *American journal of disaster medicine*, vol. 3, no. 2, pp. 87–97, 2007.

[9] R. R. Murphy, K. L. Dreger, S. Newsome, J. Rodocker, E. Steimle, T. Kimura, K. Makabe, F. Matsuno, S. Tadokoro, and K. Kon, "Use of remotely operated marine vehicles at minamisanriku and rikuzentakata japan for disaster recovery," in *Proc. IEEE Int. Symp. on Safety, Security, and Rescue Robotics*, 2011, pp. 19–25.

[10] L. Moody, C. Baber, T. N. Arvanitis, *et al.*, "Objective surgical performance evaluation based on haptic feedback," *Studies in Health Technology and Informatics*, pp. 304–310, 2002.

[11] C. Pacchierotti, S. Scheggi, D. Prattichizzo, and S. Misra, "Haptic feedback for microrobotics applications: a review," *Frontiers in Robotics and AI*, vol. 3, no. 53, 2016.

[12] A. Bolopion and S. Régnier, "A review of haptic feedback teleoperation systems for micromanipulation and microassembly," *IEEE Transactions on Automation Science and Engineering*, vol. 10, no. 3, pp. 496–502, 2013.

[13] C. Pacchierotti, F. Ongaro, F. van den Brink, C. Yoon, D. Prattichizzo, D. Gracias, and S. Misra, "Steering and control of miniaturized untethered soft magnetic grippers with haptic assistance," *IEEE Transactions on Automation Science and Engineering. In Press*, 2017.

[14] C. Pacchierotti, M. Abayazid, S. Misra, and D. Prattichizzo, "Tele-operation of steerable flexible needles by combining kinesthetic and vibratory feedback," *IEEE Transactions on Haptics*, vol. 7, no. 4, pp. 551–556, 2014.

[15] J. Abbott, P. Marayong, and A. Okamura, "Haptic virtual fixtures for robot-assisted manipulation," *Robotics Research*, pp. 49–64, 2007.

[16] A. Peer and M. Buss, "A new admittance-type haptic interface for bimanual manipulations," *IEEE/ASME Transactions on Mechatronics*, vol. 13, no. 4, pp. 416–428, 2008.

[17] J. C. Gwilliam, M. Mahvash, B. Vagvolgyi, A. Vacharat, D. D. Yuh, and A. M. Okamura, "Effects of haptic and graphical force feedback on teleoperated palpation," in *Proc. IEEE Int. Conf. on Robotics and Automation*, 2009, pp. 677–682.

[18] C. Pacchierotti, D. Prattichizzo, and K. J. Kuchenbecker, "Cutaneous feedback of fingertip deformation and vibration for palpation in robotic surgery," *IEEE Transactions on Biomedical Engineering*, vol. 63, no. 2, pp. 278–287, 2016.

[19] C. Pacchierotti, L. Meli, F. Chinello, M. Malvezzi, and D. Prattichizzo, "Cutaneous haptic feedback to ensure the stability of robotic teleoperation systems," *International Journal of Robotics Research*, vol. 34, no. 14, pp. 1773–1787, 2015.

[20] D. Prattichizzo, C. Pacchierotti, and G. Rosati, "Cutaneous force feedback as a sensory subtraction technique in haptics," *IEEE Transactions on Haptics*, vol. 5, no. 4, pp. 289–300, 2012.

[21] C. R. Wagner, N. Stylopoulos, and R. D. Howe, "The role of force feedback in surgery: analysis of blunt dissection," in *Proc. 10th Symposium of Haptic Interfaces for Virtual Environment and Teleoperator Systems*, 2002, pp. 68–74.

[22] H. Culbertson and K. Kuchenbecker, "Importance of matching physical friction, hardness, and texture in creating realistic haptic virtual surfaces," *IEEE Transactions on Haptics. In Press*, 2016.

[23] D. Prattichizzo, F. Chinello, C. Pacchierotti, and M. Malvezzi, "Towards wearability in fingertip haptics: a 3-dof wearable device for cutaneous force feedback," *IEEE Transactions on Haptics*, vol. 6, no. 4, pp. 506–516, 2013.

[24] A. Girard, M. Marchal, F. Gosselin, A. Chabrier, F. Louveau, and A. Lécuyer, "Haptip: Displaying haptic shear forces at the fingertips for multi-finger interaction in virtual environments," *Frontiers in ICT*, vol. 3, p. 6, 2016.

[25] C. Pacchierotti, A. Tirmizi, G. Bianchini, and D. Prattichizzo, "Enhancing the performance of passive teleoperation systems via cutaneous feedback," *IEEE Transactions on Haptics*, vol. 8, no. 4, pp. 397–409, 2015.

[26] C. Pacchierotti, S. Sinclair, M. Solazzi, A. Frisoli, V. Hayward, and D. Prattichizzo, "Wearable haptic systems for the fingertip and the hand: Taxonomy, review, and perspectives," *IEEE Transactions on Haptics*, vol. PP, no. 99, pp. 1–1, 2017.

[27] J. M. Romano, S. R. Gray, N. T. Jacobs, and K. J. Kuchenbecker, "Toward tactilely transparent gloves: Collocated slip sensing and vibrotactile actuation," in *Proc. World Haptics*, 2009, pp. 279–284.

[28] L. Hayes, "Vibrotactile feedback-assisted performance," in *Proc. New Interfaces for Musical Expression*, 2011, pp. 72–75.

[29] Y. Kurihara, T. Hachisu, K. J. Kuchenbecker, and H. Kajimoto, "Jointonation: robotization of the human body by vibrotactile feedback," in *SIGGRAPH Asia 2013 Emerging Technologies*, 2013, p. 11.

[30] A. Brygo, I. Sarakoglou, N. Tsagarakis, and D. G. Caldwell, "Tele-manipulation with a humanoid robot under autonomous joint impedance regulation and vibrotactile balancing feedback," in *2014 IEEE-RAS Int. Conf. on Humanoid Robots*, Nov 2014, pp. 862–867.

[31] A. Hein and M. Brell, "contact-a vibrotactile display for computer aided surgery," in *Proc. World Haptics*, 2007, pp. 531–536.

[32] J. S. Zelek, S. Bromley, D. Asmar, and D. Thompson, "A haptic glove as a tactile-vision sensory substitution for wayfinding." *Journal of Visual Impairment & Blindness*, vol. 97, no. 10, pp. 1–24, 2003.

[33] J. Foottit, D. Brown, S. Marks, and A. M. Connor, "An intuitive tangible game controller," in *Proc. Conference on Interactive Entertainment*, 2014, pp. 1–7.

[34] A. Mazzoni and N. Bryan-Kinns, "Mood glove: A haptic wearable prototype system to enhance mood music in film," *Entertainment Computing*, 2016.

[35] M. G. Catalano, G. Grioli, E. Farnioli, A. Serio, C. Piazza, and A. Bicchi, "Adaptive synergies for the design and control of the pisa/iit softhand," *The International Journal of Robotics Research*, vol. 33, no. 5, pp. 768–782, 2014.

[36] R. Smits, "KDL: Kinematics and Dynamics Library," orocos.org/kdl.

[37] S. R. Buss, "Introduction to inverse kinematics with jacobian transpose, pseudoinverse and damped least squares methods," 2004.

[38] D. Prattichizzo and J. Trinkle, "Chapter 28 on grasping," in *Handbook on Robotics*, B. Siciliano and O. Kathib, Eds. Springer, 2008, pp. 671–700.

[39] D. Bassily, C. Georgoulas, J. Guettler, T. Linner, and T. Bock, "Intuitive and adaptive robotic arm manipulation using the leap motion controller," in *ISR/Robotik 2014; 41st International Symposium on Robotics; Proceedings of*, 2014, pp. 1–7.

[40] A. De Luca and R. Mattone, "Sensorless robot collision detection and hybrid force/motion control," in *Proc. IEEE international conference on robotics and automation*, 2005, pp. 999–1004.

[41] A. De Luca, A. Albu-Schaffer, S. Haddadin, and G. Hirzinger, "Collision detection and safe reaction with the DLR-III lightweight manipulator arm," in *Proc. IEEE/RSJ Int. Conf. on Intelligent Robots and Systems*, 2006, pp. 1623–1630.

[42] B. Siciliano and L. Villani, "Robot force control," 2012.

[43] M. Linderoth, A. Stolt, A. Robertsson, and R. Johansson, "Robotic force estimation using motor torques and modeling of low velocity friction disturbances," in *Intelligent Robots and Systems (IROS), 2013 IEEE/RSJ International Conference on*. IEEE, 2013, pp. 3550–3556.

[44] W. H. Ahrens, D. J. Cox, and G. Budhwar, "Use of the arcsine and square root transformations for subjectively determined percentage data," *Weed Science*, pp. 452–458, 1990.